New method to improve the grain alignment and performance of thermoelectric ceramics

N.M. Ferreira[1,*], Sh. Rasekh[2], F.M. Costa[1], M.A. Madre[2], A. Sotelo[2], J.C. Diez[2], M. A. Torres[3]

[1] i3N, Departmento de Física, Universidade de Aveiro, 3810-193 Aveiro, Portugal
[2] Instituto de Ciencia de Materiales de Aragón (CSIC-Universidad de Zaragoza), Mª de Luna, 3. 50018 Zaragoza, Spain.
[3] Departamento de Ingeniería de Diseño y Fabricación, Universidad de Zaragoza, Mª de Luna, 3. 50018 Zaragoza, Spain.
* nmferreira@ua.pt

Abstract

Textured $Bi_2Ca_2Co_{1.7}O_x$ ceramic rods were obtained by Electrically Assisted Laser Floating Zone (EALFZ) technique. The polarity effects of an external current, applied during the laser floating zone growth, have been investigated. Microstructure and thermoelectric properties have been studied and correlated with the current polarity. An important improvement of power factor was obtained for samples grown with the positive pole connected to the seed. This result evidences the advantages of EALFZ technique as a potential method for obtaining high performance thermoelectric materials.

Keywords

Texturing; thermoelectrics ceramics; Electrical properties; Thermopower

1. Introduction

In the past two decades, from the discovery of the first ceramic thermoelectric material, lots of efforts have been done in order to obtain high performance thermoelectric materials for their application on energy conversion systems [1]. Among these materials, cobaltite oxide ceramics have attracted great attention due to their performance, especially at high temperature, where conventional semiconductor base thermoelectric modules can lose their properties due to degradation, oxidation, and/or evaporation [2].

Various approaches have been made to obtain bulk samples with thermoelectric properties as close as possible to the single crystal ones, such as template grain growth (TGG) [3], uniaxial hot pressing (HP) [4], spark plasma sintering [5] or directional solidification from the melt [6]. Among these last techniques, the laser floating zone (LFZ) has shown a high reliability to obtain thermoelectric ceramics with improved electrical properties [6].

The LFZ method has also proven to be a very effective technique to produce textured ceramic materials but it must be taken into account that the obtained grain alignment strongly depends on the growth rate [6,7]. Therefore, in order to obtain very highly textured materials, low growth rates are usually needed, which, in fact, limit the practical application of this technique. As a consequence, great efforts have been done to optimize the relationship between grain alignment and pulling rate. In previous works it has been reported a significant grain alignment improvement by the laser floating zone method under the application of an external DC electrical current, the so-called electrically assisted laser floating zone (EALFZ) method [8-12]. The application of the EALFZ method on the Bi-Sr-Ca-Cu-O superconducting materials revealed a strong dependence of transport properties on electrical polarization [8-11]. A direct current (positive pole connected to the seed rod) led to stronger grain alignment, resulting on an improvement of the critical current density.

In the present work, the authors applied, for the first time, the EALFZ technique to the $Bi_2Ca_2Co_{1.7}O_x$ thermoelectric ceramic materials. For such purpose, the effects of an external DC current polarization on phase development, microstructure and thermoelectric properties of Bi-Ca-Co-O ceramic have been studied.

2. Experimental

Polycrystalline $Bi_2Ca_2Co_{1.7}O_x$ materials were prepared using the conventional solid-state synthesis technique from commercial Bi_2O_3 (Panreac, 98%), $CaCO_3$ (Panreac, 98%) and Co_2O_3 (Aldrich, 98%) powders. They were weighed in the appropriate proportions, mixed, milled and thermally treated twice at 750 and 800ºC for 12h under air, with an intermediate milling. The thermally treated powders were then isostatically cold pressed at 200MPa to obtain green ceramic cylinders which were subsequently used as feed in a LFZ device equipped with a continuous CO_2 Spectron SLC laser (10.6μm) and an external dc power supply ISO TECH IPS 603. The texturing processes have been performed at the same growth rates, 30mm/h, for all the samples, as it is schematically indicated in Figure 1. At the same time that the growth processes were performed, dc current intensities of +100 (direct) and -100mA (reverse) were applied to the growth system (+ and - indicate the connected pole to the seed). Furthermore, some other samples were grown without applying electrical current in order to be used as reference.

The as-grown samples were structurally characterized by XRD analysis performed on powdered fibres samples using a Philips X'Pert MRD equipment between 10 and 40 degrees. Microstructures have been recorded using a scanning electron microscope (SEM, Hitachi SU 70) provided with an energy dispersive spectroscopy (EDS) system used to analyse phases composition. Micrographs of longitudinal polished sections of the samples have been observed to qualitatively determine the amount of phases and their distribution using Digital Micrograph software.

Electrical resistivity (ρ) and thermopower (S) were simultaneously determined by the standard dc four-probe technique in a LSR-3 measurement system (Linseis GMBh). The samples were measured in the steady state mode at temperatures ranging from 50 to 650°C, under He atmosphere. With the electrical resistivity and thermopower data, the power factor ($PF=S^2/\rho$) has been calculated in order to establish the performance of the different samples.

Results and discussion

Powder XRD patterns for the samples obtained from the $Bi_2Ca_2Co_{1.7}O_x$ precursors and grown with the different electric fields are displayed in Figure 2. In this plot, it can be clearly seen that the ceramics grown without or with direct current (+100mA) show very similar patterns (see Figure 2a and b). In both cases, the most intense peaks have been assigned to the $Bi_2Ca_2Co_{1.7}O_x$ thermoelectric phase [13]. The diffraction planes corresponding to this phase are indicated in Figure 2a. In addition to this phase, a small amount of other secondary phases have also been identified (✶ in Figure 2a), such as $Bi_6Ca_4O_{13}$, with C2mm space group [14].

When a direct electrical current (+100 mA) is applied during the crystallization process, some changes can be observed in the XRD plot: the non-thermoelectric phase $Bi_6Ca_4O_{13}$ amount significantly decreases (see Figure 2b), while a new phase, $Ca_3Co_4O_9$, is formed (+). For the samples grown with reverse current (-100mA), the XRD pattern is radically different to the other two (see Figure 2c): the thermoelectric $Bi_2Ca_2Co_{1.7}O_x$ phase disappears and a large number of secondary non-thermoelectric phases are developed, such as CaO [15], Co_3O_4 [16], Bi_3CaO_5 [17], $Bi_6Ca_4O_{13}$ [14], $Bi_6Ca_7O_{16}$ [18] and metallic Bi [19].

The phase evolution observed in X-ray diffraction study was confirmed by the energy dispersive spectroscopy analysis made in the scanning electron microscope. In the SEM micrographs shown in Figure 3, it can be clearly seen the differences on microstructure produced by the solidification under an electrical current and those grown without it. Furthermore, it can be easily observed the effect of current polarity on the obtained microstructures. In Figure 3a, the microstructure of samples grown without applied electrical current show three different contrasts, associated by EDS to three different phases: Co_3O_4 (black contrast, #1), $Bi_6Ca_4O_{13}$ (white, #2), and $Bi_2Ca_2Co_{1.7}O_x$ (grey, #3). The thermoelectric grains (grey contrast) tend to be aligned with the rod axis due to the high thermal gradient at the solidification interface. When the crystallization process is performed under a direct current (see Figure 3b) the grain alignment is significantly improved. Moreover, the amount of thermoelectric phase is increased together with an important reduction on the non-thermoelectric (from

3 to less than 1vol.% for Co_3O_4, and 50 to around 25vol.% for $Bi_6Ca_4O_{13}$) phases and the formation of a new phase ($Ca_3Co_4O_9$, long dark grey grains, #4, appearing in about 5vol.%). This behaviour has already been observed in Bi-Sr-Ca-Cu-O superconducting materials grown by the EALFZ method [8,9,11].

On the other hand, when the samples are grown under reverse current (-100mA), no thermoelectric phase can be observed, in clear agreement with the XRD results. Furthermore, the formed non thermoelectric phases (already identified by XRD) do not show any preferential grain alignment (see Figure 3c). Another interesting feature which can be found in these samples is illustrated in Figure 3d where globular excrescences, with Bi_2O_3 composition, can be observed. The very different microstructure and phases obtained under reverse current can be explained from an electrochemical point of view. When samples are grown under these conditions bismuth oxide is reduced to metallic bismuth due to its higher value of standard electrode potentials (+0.208V) when compared to the ones for cobalt (-0.208V) or calcium (-2.868V) oxides [20], which explains the metallic bismuth found in the centre of the samples (in agreement with the XRD data). Moreover, some of the liquid Bi can be expelled off the molten zone forming the globular excrescences found on the solidified samples which will superficially oxidized in contact with the surrounding atmosphere.

The measured thermoelectric properties are shown in Figure 4 for samples grown with and without direct current. For samples grown under reverse current, no thermoelectric properties have been obtained, confirming the XRD data and SEM observations. As it can be seen in Figure 4a, an important reduction on the electrical resistivity is obtained when direct current is applied in the growth process. This effect is due to the better grain alignment and bigger thermoelectric grains sizes, as well as the reduction of non thermoelectric secondary phases, in agreement with previously discussed results. On the other hand, the measured thermopower values are slightly lower than the obtained for samples grown with no applied current (see Figure 4a), which is an expected result taking into account the reduction on the electrical resistivity [6,7].

In order to evaluate the thermoelectric performances of these different samples, the power factor has been calculated. The temperature dependence of PF, calculated from the resistivity and thermopower values represented in Figure

4a, is plotted in Figure 4b. When considering PF values at around 50ºC (~room temperature), it can be clearly seen that samples grown without applied current have values around 0.055mW/K^2 m, slightly higher than the obtained for samples grown with a Nd:YAG (λ=1.06 μm) powered LFZ system (~ 0.048mW/K^2m) [21] due to the different radiation-matter interaction, which is in agreement with previous results obtained in superconducting ceramics [22]. For samples grown with applied current, an important raise on the PF values is found (~0.088mW/K^2m) due to the high decrease on the electrical resistivity. Moreover, at 650ºC, the obtained PF is about two times higher than the obtained in similar textured composition [23].

Conclusions

In summary, it has been evidenced that the application of an external electrical current during LFZ growth strongly influences the crystallization processes which, in turn, determine the grain orientation and sizes of the thermoelectric phase. Moreover, it is also responsible of the amount and type of secondary phases. As a consequence, controlling the microstructure modifications, it is possible to maximize the measured thermoelectric properties. On the other hand, when the negative electrode is connected to the seed, thermoelectric phase cannot be formed, leading to non-thermoelectric materials.

The EALFZ technique has been proven to be an effective route to enhance the grain orientation and, as a consequence, reducing in an important manner the electrical resistivity of cobaltite materials, when a direct polarization is applied. In spite of a slight decrease on the thermopower values, the power factor values obtained in these samples are around 50% higher than those measured on samples grown without applied current.

Acknowledgments

The work was supported by the cooperation projects: E-41/11 and AIB2010-PT-00247.

Sh. Rasekh acknowledges a JAEPre-2010 fellowship from the CSIC.

A. Sotelo, M. A. Madre, J. C. Diez, and Sh. Rasekh acknowledge the MICINN-FEDER (Project MAT2008-00429), Universidad de Zaragoza (UZ2011-TEC-03), and Gobierno de Aragon (Grupos de Investigacion consolidados T12 and T87) funding.

The authors gratefully acknowledge Marta Ferro for her assistant on SEM/EDS analysis, using the equipment supported by FCT Project REDE/1509/RME/2005.

The authors acknowledge the financial support from the Portuguese Science and Technology Foundation (FCT) through the program PEst-C/CTM/LA0025/2011.

References

[1] I. Terasaki, Y. Sasago, K. Uchinokura, Phys. Rev. B 56 (1997) 12685.

[2] D. M. Rowe, Thermoelectrics Handbook: Macro to Nano, first ed., CRC Press, Boca Raton, Fl., 2006.

[3] E. Guilmeau, M. Mikami, R. Funahashi, D. Chateigner, J. Mater. Res. 20 (2005) 1002.

[4] Y. Masuda, D. Nagahama, H. Itahara, T. Tani, W.S. Seo, K. Koumoto, J. Mater. Chem. 13 (2003) 1094.

[5] J. Noudem, J. Eur. Ceram. Soc. 29 (2009) 2659.

[6] J. C. Diez, E. Guilmeau, M. A. Madre, S. Marinel, S. Lemonnier, A. Sotelo, Solid State Ionics 180 (2009) 827.

[7] A. Sotelo, E. Guilmeau, M. A. Madre, S. Marinel, S. Lemonnier, J. C. Diez, Bol. Soc. Esp. Ceram. V. 47 (2008) 225.

[8] M. F. Carrasco, R. F. Silva, J. M. Vieira, F. M. Costa, Supercond. Sci. Technol. 17 (2004) 612.

[9] M. F. Carrasco, V. S. Amaral, J. M. Vieira, R. F. Silva, F. M. Costa, Supercond. Sci. Technol. 19 (2006) 15.

[10] F. M. Costa, M. F. Carrasco, N. Ferreira, R. F. Silva, J. M. Vieira, Physica C 408–410 (2004) 915.

[11] F. M. Costa, M. F. Carrasco, R. F. Silva, J. M. Vieira, High Tc Superconducting Fibers Processed by Conventional and Electrical Assisted Laser Floating zone, in P. S. Lewis (Ed.), Perspectives on Superconductivity Research, Nova Science Publishers, 2007, pp 35-60.

[12] R. A. Silva, F. M. Costa, R. F. Silva, J. P. Andreeta, A. C. Hernandes, J. Crystal Growth 310 (2008) 3568.

[13] A. Sotelo, E. Guilmeau, Sh. Rasekh, M. A. Madre, S. Marinel, J. C. Diez, J. Eur. Ceram. Soc. 30 (2010) 1815.

[14] J. B. Parise, C. C. Torardi, Myunghwan Whangbo, C. J. Rawn, R. S. Roth, B. P. Burton, Chem. Mater. 2 (1990) 454.

[15] J. Yamashita, S. Asano, J. Phys. Soc. Jpn. 52 (1983) 3506.

[16] X. Liu, C. T. Prewitt, Phys. Chem. Miner. 17 (1990) 168.

[17] M. Troemel, L. Martin, E. Munch, ICDD ref. 00-040-0317 (2011).

[18] M. Troemel, L. Martin, E. Munch, ICDD ref. 00-042-1454 (2011).

[19] R. Sailer, G. McCarthy, ICDD ref. 00-044-1246 (2011).

[20] Petr Vanýsek, Electrochemical Series, in David R. Lide (Ed.), CRC Handbook of Chemistry and Physics 90th Edition, CRC Press, Boca Ratón, Fl., 2009, pp. 8_20-8_29

[21] J. C. Diez, Sh. Rasekh, M. A. Madre, E. Guilmeau, S. Marinel, A. Sotelo, J. Electronic Mater. 39 (2010) 1601.

[22] G. F. de la Fuente, J. C. Diez, L. A. Angurel, J. I. Peña, A. Sotelo, R. Navarro. Adv. Mater. 7 (1995) 853.

[23] Sh. Rasekh, M. A. Madre, A. Sotelo, E. Guilmeau, S. Marinel, J. C.Diez, Bol. Soc. Esp. Ceram. V. 49 (2010) 89.

Figure Caption

Figure 1 – Scheme of current application on the Electrically Assisted Laser Floating Zone (EALFZ) method.

Figure 2 – Powder XRD spectra of $Bi_2Ca_2Co_{1.7}O_x$ nominal composition samples grown by EALFZ under: a) 0 mA, b) +100 mA, c) -100 mA. * identify the BiCaO phase, and + $Bi_6Ca_4O_{13}$ one.

Figure 3 – SEM micrographs performed on longitudinal polished rods grown by EALFZ under: a) 0 mA; b) +100 mA; c) -100 mA. d) Superficial micrograph showing the globular excrescences formed in samples grown with -100 mA. Numbers indicate the different phases: 1) Co_3O_4; 2) Bi-Ca-O; 3) $Bi_2Ca_2Co_{1.7}O_x$; 4) $Ca_3Co_4O_9$; 5) CaO; 6) Bi; and 7)

Figure 4 – Thermoelectric measurements of samples grown with: ■ = +100 mA; ● = 0 mA. Left: Electrical resistivity (symbols and line) and Thermopower (symbols); Right: Power factor.

Figure 1

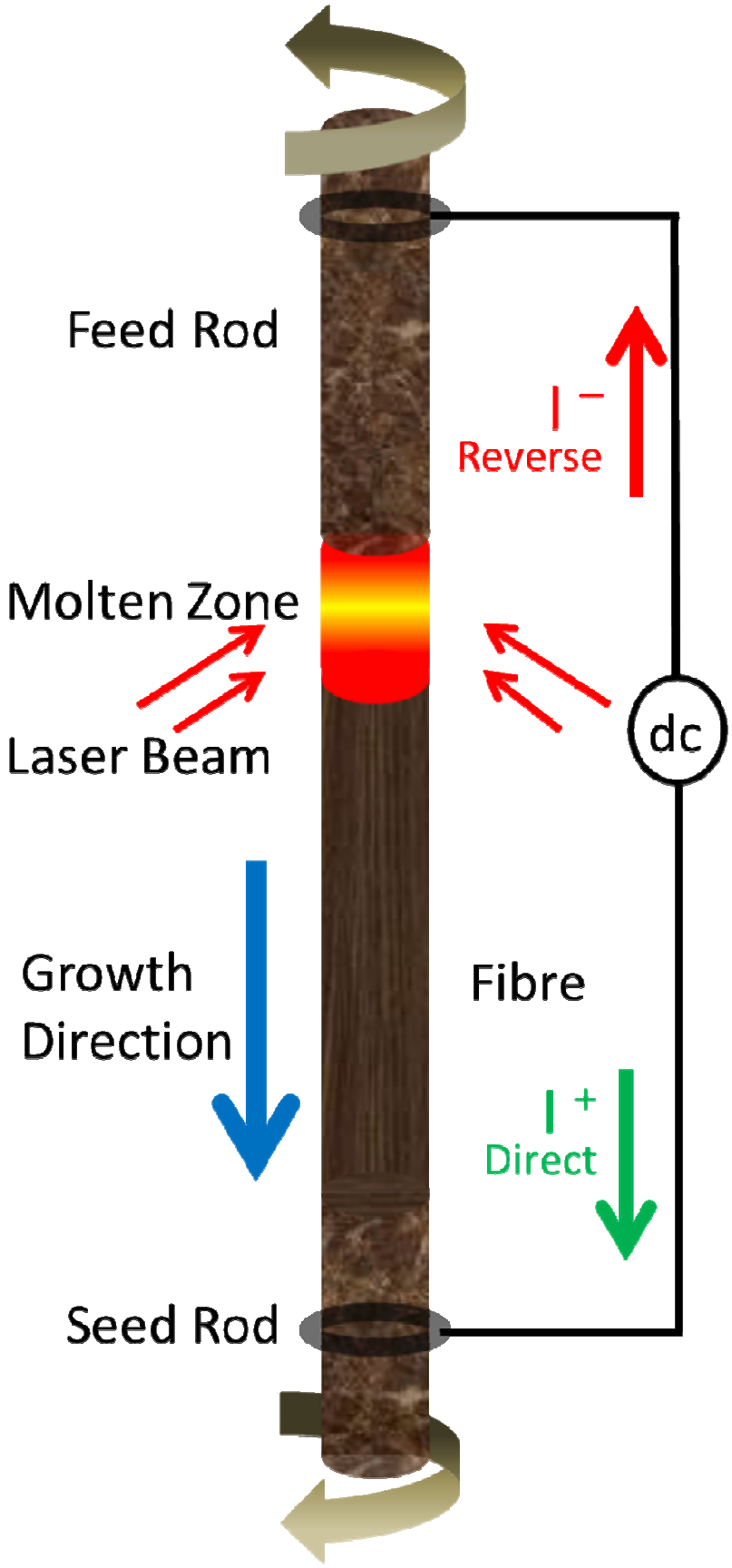
Feed Rod
I −
Reverse
Molten Zone
Laser Beam
dc
Growth
Direction
Fibre
I +
Direct
Seed Rod

Figure 2

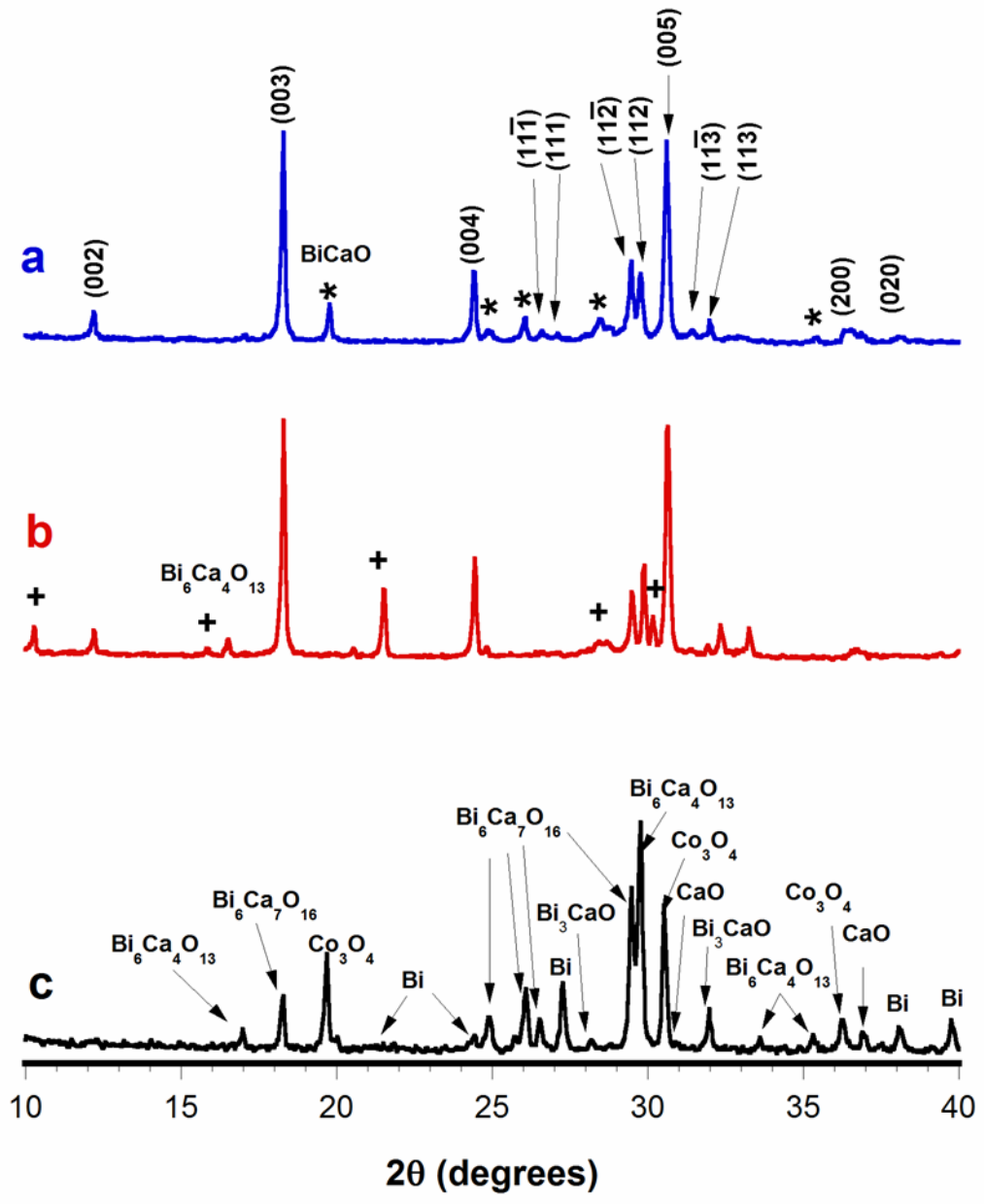
a
(002)
(003)
BiCaO
(004)
(11$\bar{1}$)
(111)
(11$\bar{2}$)
(112)
(005)
(11$\bar{3}$)
(113)
(200)
(020)
b
$Bi_6Ca_4O_{13}$
c
$Bi_6Ca_4O_{13}$
$Bi_6Ca_7O_{16}$
Co_3O_4
Bi
Bi_3CaO
CaO
10
15
20
25
30
35
40
2θ (degrees)

Figure 3

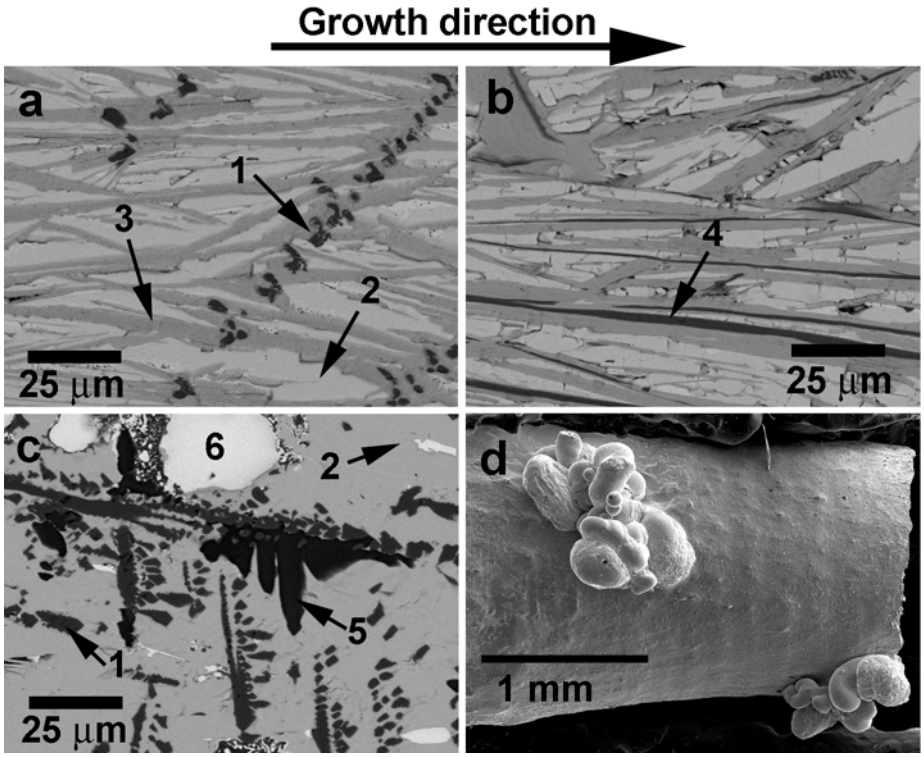

Figure 4

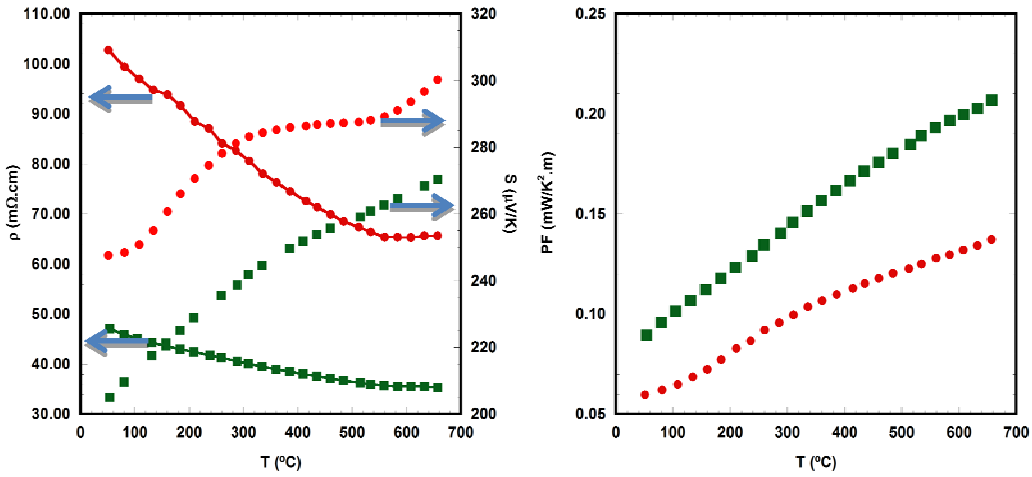
110.00
100.00
90.00
80.00
70.00
60.00
50.00
40.00
30.00
ρ (mΩ.cm)
320
300
280
260
240
220
200
S (μV/K)
0
100
200
300
400
500
600
700
T (°C)
0.25
0.20
0.15
0.10
0.05
PF (mW/K².m)
0
100
200
300
400
500
600
700
T (°C)